

Top quark mass measurement in radiative events at electron-positron colliders

M. Boronat, E. Fullana, J. Fuster, P. Gomis,^{*} and M. Vos
Institut de Física Corpuscular (Universitat de València/CSIC)

A. H. Hoang
*University of Vienna, Faculty of Physics and
 Erwin Schrödinger International Institute for Mathematical Physics*

A. Widl
University of Vienna, Faculty of Physics

V. Mateu
*Departamento de Física Fundamental e IUFFyM, Universidad de Salamanca and
 Instituto de Física Teórica UAM-CSIC*

(Dated: March 18, 2022)

In this letter, we evaluate potential of linear e^+e^- colliders to measure the top quark mass in radiative events and in a suitable short-distance scheme. We present a calculation of the differential cross section for production of a top quark pair in association with an energetic photon from initial state radiation, as a function of the invariant mass of the $t\bar{t}$ system. This *matched* calculation includes the QCD enhancement of the cross section around the $t\bar{t}$ production threshold and remains valid in the continuum well above the threshold. The uncertainty in the top mass determination is evaluated in realistic operating scenarios for the Compact Linear Collider (CLIC) and the International Linear Collider (ILC), including the statistical uncertainty and the theoretical and experimental systematic uncertainties. With this method, the top quark mass can be determined with a precision of 110 MeV in the initial stage of CLIC, with 1 ab^{-1} at $\sqrt{s} = 380 \text{ GeV}$, and with a precision of approximately 150 MeV at the ILC, with $L = 4 \text{ ab}^{-1}$ at $\sqrt{s} = 500 \text{ GeV}$. Radiative events allow measurements of the top quark mass at different renormalization scales, and we demonstrate that such a measurement can yield a statistically significant test of the evolution of the MSR mass $m_t^{\text{MSR}}(R)$ for scales $R < m_t$.

I. INTRODUCTION

The top quark plays an important role in the Standard Model (SM) and in many of its extensions. The lifetime of the top-quark ($\sim 10^{-25} \text{ s}$) is shorter than the typical timescale to form hadrons. The large decay width cuts off many of the non-perturbative QCD effects in top quark production and decay. Therefore, many top quark properties can be related with high precision to predictions in perturbation theory. That makes the top quark ideal for precise tests of the SM.

The top quark mass and the relevant entries in the CKM matrix are not predicted by the SM and must be determined experimentally. Direct top quark mass measurements at the Tevatron and the LHC experiments have reached approximately 500 MeV precision [1–3] and yield the current direct measurement world average: $m_t = 172.9 \pm 0.4 \text{ GeV}$ [4]. The experimental uncertainties of direct top mass measurements are expected to improve to approximately 200 MeV at the HL-LHC [5]. At this time it is not yet clear how the top mass value from direct measurements is related to field-theoretically defined top mass schemes, but theoretical work is on-

going to clarify the relation [6, 7]. Pole mass extractions from (differential) cross-section measurements at the LHC have quickly improved in recent years. While the latest world average from cross section measurements ($m_t^{\text{pole}} = 173.1 \pm 0.9 \text{ GeV}$ [4]) yields a consistent result, recent precision measurements [8, 9] pose some tension with the direct measurements. At electron-positron colliders, a very precise measurement of the top quark mass, with a total uncertainty of around 50 MeV and a rigorous interpretation of the measurement with respect to mass renormalization schemes, is possible by scanning the center-of-mass energy through the $t\bar{t}$ production threshold [10–12].

This letter assesses the potential of future electron-positron colliders to measure the top quark mass in associated production of a top quark pair with an energetic photon. The method we propose reconstructs the differential cross section as a function of the invariant mass $\sqrt{s'}$ of the $t\bar{t}$ system. The radiated hard photon reduces the invariant mass available for top-antitop pair production, and the spectrum develops a strong dependence on the top quark mass, as the invariant mass of the $t\bar{t}$ pair approaches the strong interaction production threshold. Such a measurement can be performed in continuum $t\bar{t}\gamma$ production at any center-of-mass energy above the $t\bar{t}$ production threshold and does not require a dedicated $t\bar{t}$ threshold run of the experiment. The extraction of the mass is robust, as it is based on an inclusive $t\bar{t}$ selection,

^{*} corresponding author: pablo.gomis@ific.uv.es

while the observable depends only on a reconstruction of the photon energy. The method furthermore offers a rigorous interpretation of the extracted top quark mass in terms of short-distance renormalization schemes, as the differential cross section can be calculated with high precision and the measurement is *inclusive* in the top quark decay products.

The analysis is based on a calculation for associated production of a top quark pair with an energetic photon radiated from the initial electron-positron pair. We derive a factorization theorem that relates the $t\bar{t}\gamma_{\text{ISR}}$ differential cross section to the total hadronic cross section $\sigma(e^+e^- \rightarrow t\bar{t}X) \equiv \sigma_{t\bar{t}}$, evaluated at the invariant mass of the hadronic $t\bar{t}X$ system. The factorization is valid at leading order in the electromagnetic coupling α_{em} and evaluated in the vector-current approximation. In the region of the invariant mass $\sqrt{s'}$ spectrum where the highest top quark mass sensitivity arises, the ISR and the vector-current approximations are valid within a few percent, which is fully sufficient for the purpose of this paper.

For our numerical studies, the description of the vector-current induced total hadronic cross section $\sigma_{t\bar{t}}$ is based on a *matched* calculation in analogy to Ref. [13], that combines an $\mathcal{O}(\alpha_s^3)$ fixed-order (N³LO) description of $t\bar{t}$ production in the continuum [14, 15] and a renormalization group improved NNLL calculation for the $t\bar{t}$ threshold region [16]. The latter accounts for bound-state effects and the summation of large logs of the $t\bar{t}$ relative velocity. This approach yields a smooth description of the QCD enhancement of the cross section at the $t\bar{t}$ production threshold due to bound-state effects and the continuum region.

We study the potential for a top quark mass measurement in two concrete scenarios, the CLIC [17, 18] initial-stage run colliding at a center-of-mass energy of 380 GeV and the ILC [19, 20] run at 500 GeV. The statistical uncertainties are estimated for the most up-to-date operating scenarios, which envisage an integrated luminosity of 1 ab^{-1} for the CLIC initial stage [21] and 4 ab^{-1} for the ILC run [22]. We take into account a realistic experimental acceptance, selection efficiency and resolution, based on detailed simulation studies in Refs. [10, 23]. We also study the impact of the luminosity spectrum on this measurement in detail.

II. OBSERVABLE DEFINITION

We consider radiative $e^+e^- \rightarrow t\bar{t} + X + \gamma$ events, such as those depicted in the rightmost diagram of Figure 1, where a top quark pair is produced in association with an energetic photon. The momentum carried away by the radiated photon reduces the phase space available for $t\bar{t}$ -pair production.

Accounting for the photon emission the squared invari-

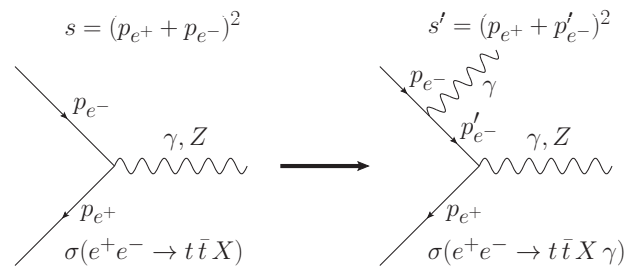


FIG. 1. Feynman diagrams representing the center-of-mass energy available for the $t\bar{t}$ -pair production before (left) and after (right) the ISR photon emission.

ant mass of the $t\bar{t}$ system s' is given by:

$$s' = s \left(1 - \frac{2E_\gamma}{\sqrt{s}} \right), \quad (1)$$

where \sqrt{s} is the nominal center-of-mass energy of the e^+e^- collider and E_γ denotes the photon energy. The differential cross section as a function of $\sqrt{s'}$ is shown in Figure 2 for a center-of-mass energy of 380 GeV and two values of the top quark mass. The maximum sensitivity of the observable is reached at the $t\bar{t}$ -pair production threshold (*radiative return* to the $t\bar{t}$ -pair production threshold).

Importantly, s' depends only on the nominal center-of-mass energy \sqrt{s} of the e^+e^- collision and the photon energy E_γ . The center-of-mass energy is precisely known and the photon energy can be measured accurately in the electromagnetic calorimeter system. The determination of s' only depends on these two quantities and is therefore under excellent experimental control. The analysis does in particular not require a detailed kinematic reconstruction of the top quark candidates.

In this method, the top quark mass is extracted from a measurement of the differential $e^+e^- \rightarrow t\bar{t}\gamma_{\text{ISR}}$ cross section with respect to s' . As can be seen in Figure 2, the sensitivity to the top quark mass mainly comes from the region where the photon energy E_γ is close to $E_{\gamma,\text{max}} = (s - 4m_t^2)/(2\sqrt{s})$, the kinematic bound for top quark pair production, where $s' \approx 4m_t^2$. In this region, the dependence of the cross section on s' shows the characteristic 1S bound state resonance enhancement. Physically, this kinematic region corresponds to the photon being radiated back-to-back to a collinear $t\bar{t}$ pair with t and \bar{t} having identical momenta. In practice, photons collinear to the incoming electron and positron beams are not accessible experimentally. Therefore, we use the cross section differential in both the photon polar angle θ and the hadronic system invariant mass $d\sigma_{t\bar{t}\gamma}/(d\cos\theta d\sqrt{s'})$, where θ is defined with respect to the direction of the incoming electron.

The polar angle θ is integrated over a range which is limited by the experimental acceptance, typically down to a polar angle $\sim 8^\circ$. Smaller angles suffer from collinear enhancements that would require resummation. The latter is not included in our theoretical setup but could be

accounted for in principle. Soft photon singularities do not arise because we only consider energetic photons with an energy $E_\gamma > 5$ GeV. The highest top mass sensitivity comes from the threshold region, far from this restriction.

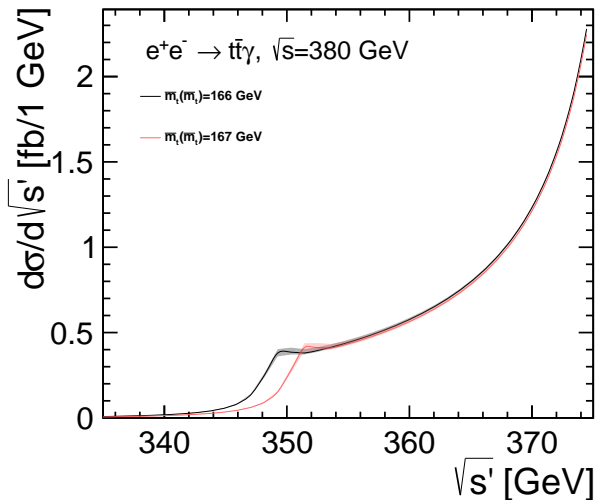


FIG. 2. Prediction of the differential cross section versus $\sqrt{s'}$ with the matched NNLL threshold and N³LO continuum calculation for vector-current induced $t\bar{t}$ production. The black and red curves correspond to two different values of the \overline{MS} mass: $\overline{m}_t(\overline{m}_t) = 166$ GeV and 167 GeV, respectively. The photon angle θ ranges from 8° to 172° and the photon energy E_γ must exceed 5 GeV.

III. THEORETICAL PREDICTION

A. Basic approximations and factorization

As can be seen in Figure 2, an accurate prediction of the s' distribution requires a *matched* calculation that provides a smooth description valid at the $t\bar{t}$ production threshold and at invariant masses $\sqrt{s'}$ well above threshold. For top mass measurements, the threshold region is essential and requires the best possible precision. For the theoretical prediction we use two essential approximations that significantly simplify the calculations. First, we only include ISR photons, and, second, we only account for vector-current induced top pair production. In the threshold region we have calculated the dominant $t\bar{t}$ S-wave Wilson coefficient and checked at tree-level that ISR diagrams (which are gauge-invariant) approximate the full Standard Model Wilson coefficient within 2.2% (and 5.2%) or better for the cross section integrated over the photon polar angles θ mentioned above at $\sqrt{s} = 380$ GeV (and 500 GeV). In the $t\bar{t}$ continuum the ISR approximation is known to be still very efficient. We note that the ISR approximation may be further improved by additional photon isolation cuts.

In the ISR approximation and at leading order in the electromagnetic coupling, one can show that the observable factorizes as follows:

$$\frac{d\sigma_{t\bar{t}\gamma}}{d\cos\theta d\sqrt{s'}} = 2g(x, \theta) \sqrt{\frac{1-2x}{s}} \frac{\alpha_{\text{em}}}{\pi} \sigma_{t\bar{t}}(s') + \mathcal{O}(\alpha_{\text{em}}^2),$$

$$x = \frac{E_\gamma}{\sqrt{s}}, \quad (2)$$

where $g(x, \theta)$ is a calculable function of the photon polar angle θ and the fraction x of the center-of-mass energy carried by the photon. The derivation of this result is presented in the Appendix and the analytic expression for g is shown in Eq. (A6).

As an additional approximation we only account for the vector-current induced contribution to $\sigma_{t\bar{t}}$. In the $t\bar{t}$ threshold region, axial-vector induced top pair production is related to P-wave $t\bar{t}$ states, which are suppressed by the square of the top velocity v (defined in the $t\bar{t}$ center-of-mass frame) with respect to the S-wave contributions induced by the vector-current. The P-wave contributions are known to be at the level of a few percent (see e.g. Ref. [24]) and therefore negligible at the level of precision of our analysis. In the continuum region, for $E_\gamma > 5$ GeV, the axial-vector induced contribution is still at the few percent level for $\sqrt{s} = 380$ GeV because $v < 0.4$. For $\sqrt{s} = 500$ GeV the axial-vector induced contribution in the continuum for $E_\gamma > 5$ GeV can reach around 10%. Since the top mass sensitivity of our method arises from the threshold region, our vector-current approximation is viable for $\sqrt{s} = 500$ GeV for the purpose of our analysis. For the analysis with real data at $\sqrt{s} = 500$ GeV, however, the axial-vector-current induced cross section contributions must be included.

B. Matched cross section

To obtain the matched vector-current induced contribution to $\sigma_{t\bar{t}}$ we proceed as follows. In the threshold region, the calculation must account for the QCD enhancement of the cross section due to non-relativistic bound-state effects. This entails that the top velocity v is an additional small expansion parameter and terms proportional to $(\alpha_s/v)^n$ [and possibly $(\alpha_s \log v)^m$] must be summed to all orders in α_s . The description of the threshold region used in this work is based on the renormalization-group-improved vNRQCD calculations of Refs. [16, 24] which include $(\alpha_s \log v)^m$ resummation and achieved NNLL (next-to-next-to-leading logarithmic) precision. The resulting QCD uncertainties are around 5% [16] and determine the theoretical uncertainties of our main numerical top mass analysis discussed in section V. The precision may be improved in future work through a combination with the N³LO fixed-order results of Ref. [25], but at this level also the ISR and vector-current approximations should be lifted by additional dedicated computations.

For the continuum region of the vector-current contribution to $\sigma_{t\bar{t}}$, where the fixed-order QCD expansion applies, we use the exact results from [26] at $\mathcal{O}(\alpha_s^{0,1})$ and the Padé approximation results at $\mathcal{O}(\alpha_s^{2,3})$ from Ref. [14], which are numerically equivalent to the corresponding results of Refs. [15, 27]. The Padé approximation uncertainties are subleading compared to renormalization scale uncertainties for our analysis, where top mass sensitivity arises mainly for $\sqrt{s'} \lesssim 380$ GeV.

The NNLL threshold results and the fixed-order $\mathcal{O}(\alpha_s^3)$ cross sections are matched using the approach of Ref. [13], originally applied to combine the NLL vNRQCD threshold and the $\mathcal{O}(\alpha_s)$ fixed-order cross sections. The matching procedure is based on the sum of both cross sections and minus an ‘expanded cross section’ that takes care of double counted terms. The vNRQCD and expanded cross sections are multiplied with a switch-off function that suppresses them away from threshold, which is crucial to achieve a smooth transition to the fixed-order cross section far away from threshold. The variation of the switch-off function parameters provides an estimate of the uncertainties inherent to the matching procedure. We have extended this method to NNLL and $\mathcal{O}(\alpha_s^3)$ and found that the uncertainty of the matching procedure systematically decreases when going to higher orders. At NNLL and $\mathcal{O}(\alpha_s^3)$ the uncertainty of the matching procedure on the cross section is smaller than its renormalization scale counterpart in the intermediate regime between threshold and continuum, where the matching procedure matters [28, 29].

C. Short-distance mass schemes

The matched cross section systematically keeps track of the dependence on the top quark mass and the proper renormalization scheme. The 1S [30–32] scheme m_t^{1S} is employed for the threshold cross section and the MSR [33, 34] scheme $m_t^{\text{MSR}}(R)$ is used for the fixed-order and the ‘expanded’ cross sections. The latter is matched to the $\overline{\text{MS}}$ scheme¹ for renormalization scales above the top mass. As the renormalization scale R for the MSR mass we adopt $R = m_t^{1S} v_*$. The quantity v_* , given in Equation 3, is a proxy for the top velocity in the $t\bar{t}$ center-of-mass frame. So the scale R is close to the center-of-mass 3-momentum of the top quarks (which smoothly depends on $\sqrt{s'}$) and the top mass. This dynamical MSR

mass scheme choice is very close to the 1S mass in the threshold region. It minimizes the size of the Coulomb singular corrections in the fixed-order results when leaving the threshold region and smoothly connects to the $\overline{\text{MS}}$ scheme in the high-energy regime, which minimizes fixed-order QCD corrections there. The relations of the three mass schemes and the MSR mass R-evolution equations are implemented at $\mathcal{O}(\alpha_s^4)$ precision using the results of Ref. [34] and the $\overline{\text{MS}}$ mass $\bar{m}_t \equiv \bar{m}_t(\bar{m}_t)$ as the matching point between the MSR and the $\overline{\text{MS}}$ mass. Throughout this paper we adopt the convention that mass values and uncertainties will be presented in the $\overline{\text{MS}}$ scheme \bar{m}_t . (More details are given in Refs. [28, 29].) Note that renormalon issues and the pole mass ambiguity [35, 36] do not play any role in our analysis which is exclusively based on short-distance mass schemes. The perturbative uncertainties in the relation between the three mass schemes we employ is at the level of 10 to 20 MeV, which also represents the principal theoretical limitation of a top mass determination based on our method, as far as the conceptual control of the mass schemes is concerned.

An interesting aspect is that measurements of the top quark mass within different s' (or E_γ) regions are sensitive to QCD dynamical effects at different length scales and thus allow for $m_t^{\text{MSR}}(R)$ top mass measurements at different R scales, in analogy to μ -dependent determinations of the strong coupling $\alpha_s(\mu)$ from processes dominated by QCD dynamics at different energy scales [4]. While the precise scheme (and renormalization scale) one picks to visualize the resulting ‘running’ parameter measurements has some degree of arbitrariness, an experimental confirmation of the scale-evolution predicted by theory – once a suitable scheme choice is made – represents a non-trivial consistency check of QCD. In this context it is also interesting to note that, as was first pointed out in Ref. [37], for renormalization scales below the quark mass, the scale evolution of a short-distance quark mass is linear in contrast to scales above the quark mass where it is logarithmic. This is realized also by the R-evolution of the MSR mass $m_t^{\text{MSR}}(R)$ matched to the $\overline{\text{MS}}$ mass [33, 34].

D. Renormalization scale uncertainties

The theoretical uncertainties (related to the unknown higher order corrections) are obtained from scale variations of the matched cross section following the approach of Ref. [13], where the scale multipliers h and f are used to coherently parametrize the variations of the hard ($\mu_H = h m_t$), soft ($\mu_S = h f m_t v_*$) and ultra-soft ($\mu_{\text{US}} = h f^2 m_t v_*^2$) scales in the threshold cross section (see also Refs. [16, 38]) and the renormalization scale of the fixed-order and expanded cross sections ($\mu_F = h m_t$)

¹ $\overline{\text{MS}}$ stands for the modified minimal subtraction scheme. The pole mass is obtained when renormalising the quark self-energy with the on-shell condition, such that fluctuations from all positive energies are absorbed into the mass. In contrast, in the $\overline{\text{MS}}$ scheme one defines counterterms such that only the $1/\epsilon$ divergences cancel, which effectively absorbs into the mass definition fluctuations larger than $\bar{m}_t(\bar{m}_t)$. The MSR mass interpolates between these two extremes, absorbing fluctuations above the scale R . The name reflects its close relation to the $\overline{\text{MS}}$ scheme and R-evolution.

around their default scales, where²:

$$v_\star = 0.05 + \left| \sqrt{(\sqrt{s'} - 2m_t + i\Gamma_t)/m_t} \right|. \quad (3)$$

The multiplier h parametrizes variations relative to m_t , and f parametrizes variations relative to v_\star . To estimate the uncertainty due to the truncation of the perturbative series, the h and f parameters are varied in the intervals quoted in Table I. In this procedure, outlined in Refs. [16, 38], the combinations of h and f are chosen such that the ultra-soft renormalization scale in the threshold cross section remains within a factor two of its default value, while h is varied between 1/2 and 2. This results in a relative uncertainty of $\pm 5\%$ for the cross section in the threshold region [16] and is the basis of the theoretical uncertainty in the top quark mass determination of our method. At this point we stress that our choice of the R scale in the running MSR mass $m_t^{\text{MSR}}(R)$ corresponds to a freedom in the choice of a renormalization scheme for the top mass parameter, but is not associated to the theoretical uncertainties, which are fully accounted for by the h and f variations.

TABLE I. Variations of the parameters h and f that determine the hard, soft, ultra-soft and fixed-order renormalization scales of the matched calculation. The nominal calculation corresponds to $h = f = 1$ and the variations follow the procedure of Refs. [16, 38]. The resulting $\sqrt{s'}$ distribution is fitted with the nominal calculation and the resulting shifts in the extracted value of \bar{m}_t are given in the third and fourth rows.

parameter variations									
h	1/2	1/2	1/2	1	1	1	2	2	2
f	2	3/2	1	1	$\sqrt{2}$	$\sqrt{1/2}$	1	3/4	1/2
resulting mass shift $\Delta\bar{m}_t$ [MeV]									
$\sqrt{s} = 380$ GeV:	-44	-46	-44	0	-1	+8	+29	+30	+45
$\sqrt{s} = 500$ GeV:	-55	-58	-54	0	-2	+12	+32	+34	+51

To assess the theoretical uncertainty in an extraction of the top quark mass, the differential cross section predictions in terms of $\sqrt{s'}$ (integrated over the photon angle) with varied scale settings are fitted with the nominal calculation (for $f = h = 1$), where the top quark mass in the latter is floated as a free parameter. The difference of the best-fit mass with respect to the nominal mass is listed in the third and fourth rows in Table I, for center-of-mass energies of 380 GeV and 500 GeV, respectively. The perturbative uncertainty in the mass extraction due to missing higher-order contributions is estimated as the envelope of all top mass variations. We find this theory uncertainty³ corresponds to ± 46 MeV at $\sqrt{s} = 380$ GeV and ± 55 MeV at $\sqrt{s} = 500$ GeV for the $\overline{\text{MS}}$ mass \bar{m}_t .

² For the top quark width we use $\Gamma_t = 1.5$ GeV.

³ This estimate is performed at the parton level, for collisions with

IV. EXPERIMENTAL STUDY

In this section we present the strategy to take into account experimental uncertainties. We rely on detailed simulation studies by the CLIC and ILC groups [10, 23] to estimate the size of the most important effects.

A. Event selection

The top quark pair production mechanism is the dominant six-fermion process for radiation events with a hard photon with $E_\gamma < E_{\gamma, \text{max}}$. With its striking signature it is readily isolated, reducing the background due to other SM processes to the few percent level [10]. Jets are reconstructed with the Valencia Lepton Collider or VLC algorithm, a sequential recombination algorithm for e^+e^- collisions with robust performance in the presence of background [39]. Jet clustering is exclusive, with the radius parameter R of the algorithm set to 1.6 and $\beta = \gamma = 0.8$. The two b -tagged jets are identified with the LCFIplus package [40], a crucial step in the selection. The selection of the lepton+jets final state [10, 23] is furthermore based on the presence of an isolated charged lepton (electron or muon)⁴. Also the fully hadronic final state can be efficiently selected [41]. No full-simulation studies are available for the di-lepton final state. No reconstruction of the kinematic properties of the top quarks is required for this analysis.

To take into account the selection efficiency, we assume an overall efficiency of 50% for $t\bar{t}\gamma$ events where the photon has an energy greater than 5 GeV and a polar angle between 8 and 172 degrees. This is definitely a conservative assumption given the results achieved in full simulation studies of the $t\bar{t}$ final state that demonstrate negligible background levels with similar or better selection efficiency [10, 23, 41]. The photon reconstruction efficiency, identification and isolation, discussed in the next section, are included in this overall efficiency and not accounted for separately.

B. Photon reconstruction

Energetic photons leave a characteristic electromagnetic shower in the silicon-tungsten EM calorimeter [42]

the nominal center-of-mass energy. The impact of the scale variations may be significantly larger when evaluated at the detector level. Reference [10] finds an uncertainty of ± 100 MeV, nearly double that at the parton level, for the CLIC luminosity spectrum. We assume in the following that the data can be corrected to the parton level before extracting the mass. This could be achieved by sub-dividing the sample using the event-by-event measurement of the visible energy in combination with a sophisticated unfolding of the data using the precisely measured luminosity spectrum. A rigorous demonstration remains for future work.

⁴ Events with hadronic τ -decays are not considered at this stage.

of the ILD [43] and CLICdet [44] detector concepts envisaged for the ILC and CLIC. They are efficiently identified by the Pandora Particle Flow package [45].

The expected energy resolution of the electromagnetic calorimeter [46] of the linear collider experiments is:

$$\sigma/E = 0.166/\sqrt{E} \oplus 1.1\%. \quad (4)$$

In the following the E_γ distribution will be binned according to this resolution and the result propagated to the $\sqrt{s'}$ distribution.

The most important limitation of the CLIC and ILC detectors for this analysis is the limited coverage in the forward and backward region. The tracking system and the main granular calorimeters extend out to a polar angle of approximately 8° . We therefore limit the acceptance of the analysis to the fiducial region $8^\circ < \theta < 172^\circ$ ($|\cos\theta| < 0.99$). As the distribution of ISR photons is very forward-peaked, this restriction implies a strong penalty. An extension of the acceptance to include the forward calorimeter systems ($4^\circ < \theta < 176^\circ$) doubles the available statistics. An extension to $2^\circ < \theta < 178^\circ$ would even quadruple it. As the forward calorimeters must deal with important background levels without the aid of the tracking system, this possibility requires a detailed study, that is left for future work.

Finally, as the calculation we use for the current analysis is based on photons from initial-state radiation, the presence of photons from final-state radiation must be suppressed⁵. The studies at the stable-particle level of Ref. [47] establish that a combination of cuts on the photon energy ($E_\gamma > 3\text{--}10\text{ GeV}$, depending on the center-of-mass energy) and the isolation angle (minimum angle with respect to the nearest particle, $\Omega_{\gamma,i} > 8^\circ$) is very effective to remove FSR photons, while retaining the sensitivity of the measurement.

The photon energy measurement is the key to the $\sqrt{s'}$ observable. The response of the electromagnetic calorimeter must be calibrated in-situ to achieve a precise control over the photon energy scale. The electron energy response can be calibrated using $Z \rightarrow e^+e^-$ decays with a statistical uncertainty smaller than 1×10^{-4} [48]. A direct handle on the photon response is found in radiative Z -boson decays (i.e. $Z \rightarrow \mu^+\mu^-\gamma$). ATLAS and CMS have applied both methods [49, 50]. Following their results, we assign a conservative uncertainty of 1×10^{-3} .

C. Luminosity spectrum

The solid curves in Figure 2 assume that the distribution of e^+e^- center-of-mass energy \sqrt{s} is a δ -function at the nominal center-of-mass energy $\sqrt{s_{\text{nom}}}$. In practice, beam energy spread leads to a non-negligible width,

while beamstrahlung causes a tail towards lower energies called the luminosity spectrum. In Figure 3 the expected luminosity spectra for the CLIC run at $\sqrt{s} = 380\text{ GeV}$ and the ILC run at 500 GeV are shown, as generated with the GUINEA-PIG program [51] for the nominal accelerator settings.

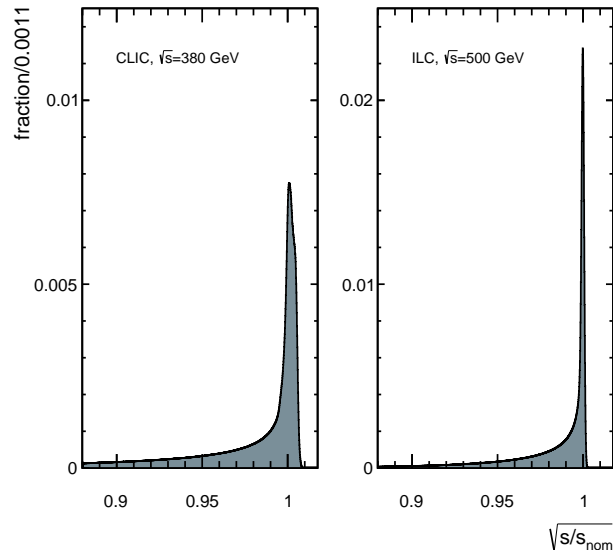


FIG. 3. The luminosity spectrum, expressed as the fraction of events per $\sqrt{s/s_{\text{nom}}}$ bin, where $\sqrt{s/s_{\text{nom}}}$ represents the center-of-mass energy of the collision relative to the nominal center-of-mass energy. The spectra correspond to CLIC at $\sqrt{s} = 380\text{ GeV}$ (left panel) and the ILC at $\sqrt{s} = 500\text{ GeV}$ (right panel).

This luminosity spectrum has an important effect on the observed $\sqrt{s'}$ distribution. Compared to the result obtained with collisions at exactly the nominal center-of-mass energy, the threshold peak gets smeared out substantially. To realize the full potential of this method the effect of the luminosity spectrum must be corrected to good accuracy. In Ref. [52] a method was developed to reconstruct the luminosity spectrum in-situ. The Bhabha scattering process $e^+e^- \rightarrow e^+e^-$, with a large cross section, simple final state, and precisely predicted angular distribution, is an ideal calibration process. Following the same approach, we have reconstructed the luminosity spectrum for CLIC380 and ILC500 by fitting a complex functional form to the Bhabha spectrum. A detailed account is found in Ref. [53]. The uncertainty in the reconstructed spectrum is estimated by varying the parameters of the fit function within their uncertainty. The effect is then propagated to the top quark mass by re-weighting the predicted spectrum with the varied luminosity spectra.

⁵ In principle, the contribution to the observable of final state photons can be added to the calculation.

TABLE II. The expected uncertainty on the top $\overline{\text{MS}}$ mass for the runs at $\sqrt{s} = 380$ GeV at CLIC and at $\sqrt{s} = 500$ GeV at the ILC. For both machines, results are presented for an integrated luminosity of 500 fb^{-1} and for the nominal operating scenario, from Ref. [17] for CLIC and Ref. [22] for the ILC.

cms energy luminosity [fb^{-1}]	CLIC, $\sqrt{s} = 380$ GeV		ILC, $\sqrt{s} = 500$ GeV	
	500	1000	500	4000
statistical	140 MeV	90 MeV	350 MeV	110 MeV
theory	46 MeV		55 MeV	
lum. spectrum	20 MeV		20 MeV	
photon response	16 MeV		85 MeV	
total	150 MeV	110 MeV	360 MeV	150 MeV

V. RESULTS

The prospects for the top quark mass determination at CLIC and the ILC are estimated using pseudo-data sets. The theoretical cross section predictions are collected in $\sqrt{s'}$ bins with a width given by the expected energy resolution of the electromagnetic calorimeter [see Eq. (4)]. For each scenario 1000 pseudo-experiments are generated by applying Poissonian fluctuations around the expected central value. The magnitude of the fluctuations reflects the expected statistical uncertainty, taking into account the production cross-section, integrated luminosity of the official run scenarios and an efficiency of 50%. The effect of the luminosity spectrum is included by folding calculations at several center-of-mass energies and weighting them according to the luminosity spectrum. Examples of pseudo-experiments are shown in Figure 4 for CLIC (left) and the ILC (right). The solid curve is the nominal prediction. The error on the pseudo-data points and the gray uncertainty band correspond to the $\pm 1\sigma$ statistical uncertainty.

The pseudo-datasets are fitted to the nominal theoretical prediction with the mass as a free parameter. The statistical uncertainty is estimated as the mean of the uncertainties provided by the TMinuit χ^2 minimization, which is in excellent agreement with the spread of the fitted mass values.

The results are presented in Table II. We find a statistical uncertainty of 90 MeV for the CLIC initial stage at $\sqrt{s} = 380$ GeV and 110 MeV for the ILC run at $\sqrt{s} = 500$ GeV. These uncertainties take into account a realistic estimate of the acceptance, selection efficiency, photon energy resolution and luminosity spectrum. For the ILC the very large integrated luminosity (4 ab^{-1}) is partly making up for the overall smaller statistics in the threshold region. For even higher energies the statistical uncertainty increases even further because of the decreasing statistics in the $t\bar{t}$ threshold region and the degraded photon energy resolution.

The impact of systematic effects on the measurement

is estimated by fitting distorted pseudo-data with the nominal calculation and registering the bias in the mass extraction. The theory uncertainty is evaluated by varying the three renormalization scales as described in section III D. The maximum upward and downward variations are taken as the uncertainty. This uncertainty amounts to approximately 50 MeV in both scenarios and is the dominant systematic uncertainty for the CLIC scenario. The uncertainty of the photon energy response is estimated by varying the energy scale up and down by one per mille. This uncertainty is quite sizable for the ILC scenario, where the photon energy is greater than 100 GeV for the threshold region. The uncertainty on the luminosity spectrum is propagated as described in section IV C and is sub-dominant in both scenarios.

VI. RUNNING OF THE TOP QUARK MASS

Measurements of $\overline{\text{MS}}$ quark masses at different energy scales have been performed on LEP data for the bottom quark [54, 55] and on HERA data for the charm quark [56]. Recently, the CMS collaboration presented the first indications for the running of the $\overline{\text{MS}}$ top quark mass at the LHC [57] for scales far above m_t . As already pointed out in section III C, the method presented in this letter allows the measurement of a scale-dependent top quark mass for scales below m_t by extracting the mass from different sections of the differential cross section as a function of $\sqrt{s'}$. As the quark mass scheme to quantify this scale-dependence we adopt the MSR mass $m_t^{\text{MSR}}(R)$, where $R = m_t^{1S} v^*$ is a proxy for the top quark 3-momenta in the $t\bar{t}$ center-of-mass frame, which is the relevant dynamical scale for the top mass dependence in inclusive top pair production (see the discussion in section III C).

Here, we present a quantitative analysis to assess the potential of the 500 GeV run envisaged by the ILC. In principle, the range of energy scales can be further extended by adding higher-energy runs. The $\sqrt{s'}$ distribution is divided in four bins. The first bin with $\sqrt{s'}/\text{GeV}$ in the interval $[339, 374]$ isolates the threshold region, with its excellent sensitivity to the top quark mass due to the rapidly varying distribution at the $1S$ resonance peak. For this bin we adopt $R = m_t^{1S} v^*(\sqrt{s'} = m_t^{1S}) = 25 \text{ GeV}$ as representative R -scale. Three further bins, $[374, 411]$, $[411, 445]$ and $[445, 495]$, provide mass measurements at higher scales. For the second bin v^* varies by $\pm 20\%$ while for the third and fourth v^* varies by $\pm 10\%$. The v^* variation is sufficiently small so that we can associate the respective mean v^* value to the representative R value for these bins. This gives $R/\text{GeV} = 94, 125$ and 153 for the second, third and fourth bin, respectively. Independent fits are carried out in each bin. The resulting fit values for $\overline{\text{MS}}$ mass $\overline{m}_t(\overline{m}_t)$ in each bin are converted to $m_t^{\text{MSR}}(R)$ at the respective representative R scale.

The expected precision of the four MSR mass measurements is indicated in Figure 5, assuming the ILC scenario with 4 ab^{-1} at $\sqrt{s} = 500$ GeV. The fit to the

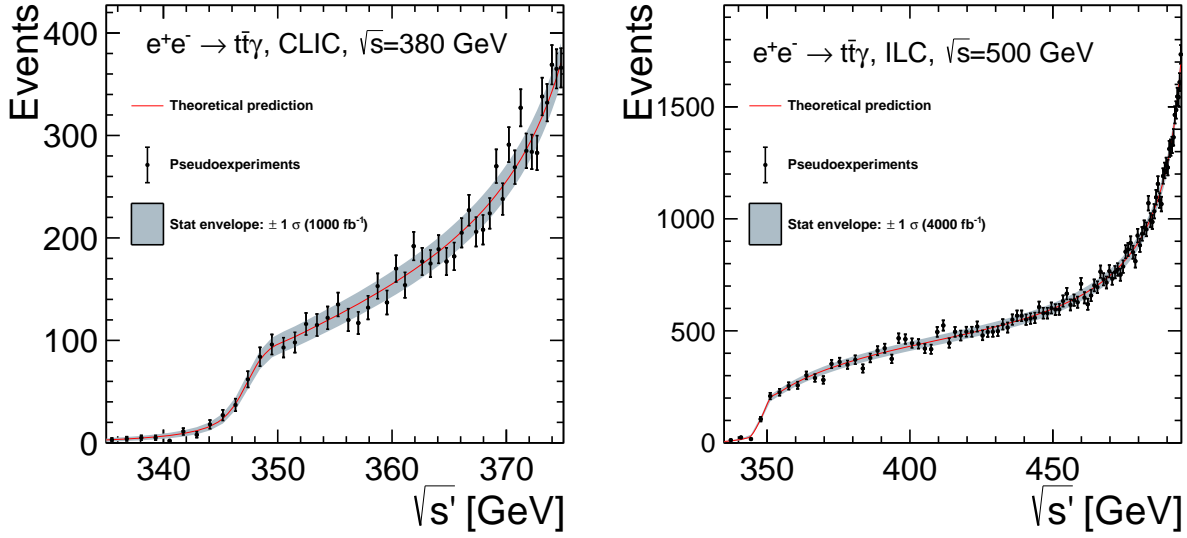


FIG. 4. Pseudodata generated with the matched NNLL threshold and $N^3\text{LO}$ continuum calculation. The left panel shows the result for $\sqrt{s} = 380$ GeV, with the CLIC luminosity spectrum, the right panel the result for $\sqrt{s} = 500$ GeV, with the ILC luminosity spectrum. The error on the pseudo-data points and the gray uncertainty band correspond to the $\pm 1\sigma$ statistical uncertainty.

bin centered on the threshold region yields a very precise measurement, with a statistical uncertainty of 110 MeV for $m_t^{\text{MSR}}(R = 25 \text{ GeV})$. At higher $\sqrt{s'}$ the sensitivity degrades very rapidly, and the statistical uncertainty of the mass measurement increases to 0.9–1.7 GeV. The theory uncertainty is indicated by blue error bars. It is evaluated at the parton-level by varying the h and f parameters that determine the hard, soft and ultra-soft scales over the range indicated in Table I. The theory uncertainty vary from 200 to 400 MeV. Experimental systematic uncertainties are smaller than this.

Taking the precise measurement at the threshold as the reference value, the difference with the results in the other bins at higher $\sqrt{s'}$ ranges from nearly 3 GeV to over 6 GeV for the R interval covered by this study. Each of these differences has a significance greater than 3σ . The overall significance is greater than 5σ . We therefore conclude that this method applied to the 500 GeV ILC data has the power to demonstrate the R-evolution of the MSR top quark mass $m_t^{\text{MSR}}(R)$ for scales $R < m_t$.

VII. SUMMARY AND CONCLUSIONS

We present a new method to measure the top-quark mass at electron-positron colliders operated at a center-of-mass energy that exceeds the top quark pair production threshold. In this method, the top quark mass is extracted from the differential distribution of $t\bar{t}\gamma$ events with respect to the invariant mass of the $t\bar{t}$ system, which is related to the photon energy. This method does not require a dedicated threshold scan at e^+e^- center-of-mass

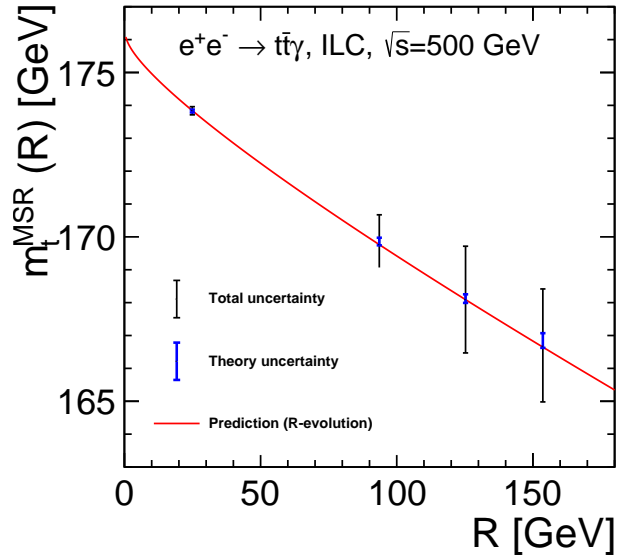


FIG. 5. Prospects for the measurement of the MSR mass evolution with the scale R . The error on the pseudo-data points is an estimate of the total uncertainty, which is dominated by the statistical uncertainty.

energies close to $2m_t$, while it can provide a mass measurement with a rigorous interpretation in terms of a field-theoretical short-distance mass scheme.

The predictions we use for the observable in our analysis are based on a factorization formula, which relies

on an ISR approximation, where we account for photon emission from the incoming electron or positron, and on a *matched* NNLL+ $\mathcal{O}(\alpha_s^3)$ QCD calculation for vector-current induced top production. This calculation provides an adequate description of the QCD enhancement of the cross section in the threshold region where the main top mass sensitivity of our method is located, so that the theoretical uncertainties of the top mass measurement can be estimated realistically, and it smoothly interpolates to the continuum region. For the continuum region our theoretical prediction is less precise, which, however, does not affect the outcome of our error analysis.

We have assessed the uncertainties that are expected for the CLIC initial stage at $\sqrt{s} = 380$ GeV and the ILC run at $\sqrt{s} = 500$ GeV. Statistical uncertainties are evaluated for realistic conditions and for the nominal operating scenarios. We also take into account a realistic estimate of the acceptance, selection efficiency, photon energy resolution and luminosity spectrum. The theory uncertainty is estimated by varying the renormalization scales in the calculation. A detailed break-down of the uncertainties is presented in Table II. With relatively modest luminosity, this method can reach a precision of the order of a few 100 MeV for the measurement of short-distance top quark mass schemes such as $\overline{\text{MS}}$ or MSR, improving the top-quark mass measurement beyond the current precision at hadron colliders. For the nominal integrated luminosity (1 ab^{-1}) a total uncertainty of 110 MeV is expected for the initial stage of CLIC at $\sqrt{s} = 380$ GeV. The ILC run at $\sqrt{s} = 500$ GeV can achieve 150 MeV with an integrated luminosity of 4 ab^{-1} .

The precision of this method is not quite competitive with that of a dedicated threshold scan [11], but can re-confirm that measurement with partially orthogonal systematic uncertainties. The method we propose can moreover access the top quark mass at various energy scales. Thus, one can test the R-evolution of the MSR top quark mass for scales $R < m_t$ (i.e. the ‘running’ of the top quark mass). The top mass extraction in several $\sqrt{s'}$ intervals with 4 ab^{-1} at $\sqrt{s} = 500$ GeV achieves sufficient precision for the observation with over 5σ significance of the evolution.

Further improvements of the method can be envisaged in several (experimental as well as theoretical) directions. The inclusion of photons detected in the forward calorimeters could extend the polar angle range of the analysis and thus reduce the statistical uncertainty. Even greater gain is possible by including associated production of a top quark pair with a jet initiated by a (final-state-radiation) gluon in the analysis. Progress in the corresponding theory approach to calculate this observable is required to bring it to a level comparable of the present analysis. Among the possible improvements of the theoretical approach we used in the present $t\bar{t}\gamma$ analysis we count: including both vector and axial-vector induced top pair production, the effects from final-state photon radiation and accounting for electroweak correc-

tions (see e.g. Refs. [58, 59] for corresponding computations for $t\bar{t}H$ production).

ACKNOWLEDGMENTS

This result could not have been obtained without the work of the CLIC and ILC collaborations to develop detailed detector concepts, and full-simulation and reconstruction software. MV acknowledges the hospitality of the CERN LCD group. The team at IFIC Valencia is supported by the Spanish national program for particle physics, projects FPA2015-65652-C4-3-R and PGC2018-094856-B-I00 (MCIU/AEI/FEDER, UE), the Severo Ochoa excellence program (SEV-2014-0398) and PROMETEO grant 2018/060 of the Generalitat Valenciana. VM is funded by the Spanish MINECO *Ramón y Cajal* program (RYC-2014-16022), the MECD grant FPA2016-78645-P and the IFT *Centro de Excelencia Severo Ochoa* Program under Grant SEV-2012-0249, and by the EU STRONG-2020 project under the program H2020-INFRAIA-2018-1, grant agreement no. 824093. AW is supported by the the FWF Doctoral Program “Particles and Interactions” No. W1252-N2. AH is supported by the FWF Austrian Science Fund under the Projects No. P28535-N27 and No. P32383-N27.

Appendix A: Derivation of the Factorization Formula

In this appendix we provide a derivation of the factorization formula shown in Eq. (2). We start by relating the total hadronic cross section to the QCD top quark current J^μ . We assume that quarks are produced directly in the interaction vertex, since secondary production is not considered in the analysis carried out in this article. We start by noting that the reduced matrix elements M_C , where $C = V, A$ denotes the vector and axial-vector current, respectively, according to the leftmost Feynman diagram shown in Fig. 1 read

$$\begin{aligned} M_C &= g_{\text{ew}}^C(s) \bar{v}(p_{e^+}) \Gamma_\mu^C u(p_{e^-}) \langle X | J_C^\mu(0) | 0 \rangle, \\ \Gamma_\mu^{\{V,A\}} &= \{\gamma_\mu, \gamma_\mu \gamma_5\}, \\ J_C^\mu(x) &= \bar{q}_t(x) \Gamma^{C\mu} q_t(x), \end{aligned} \quad (\text{A1})$$

where $g_{\text{ew}}^C(s)$ are the electroweak couplings, involving the photon and Z-boson propagators, which are different for vector and axial-vector interactions (and up-type vs down-type quarks), u and v are the lepton spinors, and q_t is the quantum field for the top quark. In the second line, the first and second entries in curly brackets correspond to vector and axial-vector currents, respectively. To compute the total hadronic cross section one has to square the reduced matrix elements (there is no interference between vector and axial-vector currents because we are totally inclusive), average over the spins of the

initial-state leptons, and sum over the polarization and phase space of the inclusive hadronic final state X . Given that we take the initial leptons as massless, the leptonic current is conserved for both vector and axial-vector interactions. Let us work out the hadronic tensors, defined as the hard matrix element squared, summed over all possible configurations:

$$\begin{aligned} W_C^{\mu\nu}(Q) &\equiv \sum_X (2\pi)^4 \delta^{(4)}(Q^\mu - p_X^\mu) \langle 0 | J_C^\mu(0)^\dagger | X \rangle \langle X | J_C^\nu(0) | 0 \rangle \\ &= B_C(s) Q^\mu Q^\nu - D_C(s) g^{\mu\nu}. \end{aligned} \quad (\text{A2})$$

Here Q^μ is the total four-momentum of either the initial or final state, such that $Q^2 = s$. The hadronic tensor can be related to the absorptive part of the vacuum polarization function. To get the last line we note that $W^{\mu\nu}$ transforms as a rank-two symmetric tensor and use the only two possible Lorentz structures that can be constructed with the momenta one has at hand. The term proportional to $Q^\mu Q^\nu$ does not contribute to the total hadronic cross section due to the effective conservation of the leptonic current. For vector interactions, current conservation of course implies the relation $D(s) = s B(s)$. To obtain the total hadronic cross section, we use this result to compute the squared matrix element, summed over all final states and averaged over initial polarization (the leptonic trace is the same for both currents), and add the flux factor $1/(2s)$:

$$\sigma_{t\bar{t}}(s) = \frac{1}{2} \sum_{C=V,A} |g_{\text{ew}}^C(s)|^2 D_C(s). \quad (\text{A3})$$

Next we consider the case of a photon with momentum p_γ radiated from the initial state leptons. The momentum flowing through the photon/Z propagator is then $Q' = Q - p_\gamma$, with $s' = (Q')^2 = s(1 - 2x)$ and x defined in Eq. (2). The reduced matrix element, according to the ISR Feynman diagram, as shown on the RHS of Fig. 1

reads

$$\begin{aligned} M_C &= g_{\text{em}} g_{\text{ew}}^C(s') F_\mu^C \langle X | J_C^\mu(0) | 0 \rangle, \\ F_\mu^C &= \bar{v}(p_{e^+}) D_\mu u(p_{e^-}), \\ D_\mu^C &= \left[\frac{\Gamma_\mu^C(\not{p}_{e^-} - \not{p}_\gamma) \gamma_\alpha}{2p_\gamma \cdot p_{e^-}} - \frac{\gamma_\alpha (\not{p}_{e^+} - \not{p}_\gamma) \Gamma_\mu^C}{2p_\gamma \cdot p_{e^+}} \right] \varepsilon^\alpha(p_\gamma), \end{aligned} \quad (\text{A4})$$

with $\varepsilon^\alpha(p_\gamma)$ the photon polarization vector. The complete phase space summation now includes also the momenta and helicity λ of the ISR photon:

$$\sum_\lambda \int \frac{d^3 \vec{p}_\gamma}{(2\pi)^3 2E_\gamma} \sum_X (2\pi)^4 \delta^{(4)}(Q^\mu - p_X^\mu - p_\gamma^\mu). \quad (\text{A5})$$

The sum over X can be performed over the product of the hadronic currents to obtain $W^{\mu\nu}(Q')$. Again the $B(s')$ Lorentz invariant term does not contribute due to the effective lepton current conservation. The leptonic trace, averaged over the lepton spins and summed over the photon helicities, is the same for vector and axial-vector currents, and we find

$$\begin{aligned} \frac{1}{4} \sum_{s_1, s_2, \lambda} F_\mu^C F^{\mu\dagger} &= -\frac{4}{x} g(x, \cos \theta), \\ g(x, \cos \theta) &= \frac{1}{x \sin^2 \theta} \left[1 - 2x + (1 + \cos^2 \theta) x^2 \right]. \end{aligned} \quad (\text{A6})$$

The radiative kernel $g(x, \cos \theta)$ exhibits both soft ($x \rightarrow 0$) and collinear [$\theta \rightarrow (0, \pi)$] singularities. With this result we can compute the differential cross section:

$$\begin{aligned} \frac{d\sigma_{t\bar{t}\gamma}}{d\cos\theta dx} &= \frac{\alpha_{\text{em}}}{\pi} g(x, \cos \theta) \sum_{C=V,A} |g_{\text{ew}}^C(s')|^2 D_C(s') \\ &= \frac{2\alpha_{\text{em}}}{\pi} g(x, \cos \theta) \sigma_{t\bar{t}}(s'), \end{aligned} \quad (\text{A7})$$

where in the last line we have used Eq. (A3) to write the result in terms of $\sigma_{t\bar{t}}$. With a trivial change of variables we obtain the result in Eq. (2). Finally, the radiative kernel can be analytically integrated over an angular bin, and this integrated kernel can be used to obtain the differential cross section of the events in which the photon ends up in a given cone.

-
- [1] ATLAS collaboration, *Measurement of the top quark mass in the $t\bar{t} \rightarrow \text{lepton} + \text{jets}$ channel from $\sqrt{s} = 8$ TeV ATLAS data and combination with previous results*, *Eur. Phys. J. C* **79** (2019) 290, [[arXiv:1810.01772](#)].
 - [2] CMS collaboration, *Measurement of the top quark mass using proton-proton data at $\sqrt{s} = 7$ and 8 TeV*, *Phys. Rev. D* **93** (2016) 072004, [[arXiv:1509.04044](#)].
 - [3] ATLAS, CDF, CMS, D0 collaboration, *First combination of Tevatron and LHC measurements of the top-quark mass*, [[arXiv:1403.4427](#)].

- [4] PARTICLE DATA GROUP collaboration, M. Tanabashi et al., *Review of Particle Physics*, *Phys. Rev. D* **98** (2018) 030001.
- [5] CMS collaboration, *Projected improvement of the accuracy of top-quark mass measurements at the upgraded LHC*, [[CMS-PAS-FTR-13-017](#)].
- [6] HL-LHC, HE-LHC WORKING GROUP collaboration, P. Azzi et al., *Standard Model Physics at the HL-LHC and HE-LHC*, [[arXiv:1902.04070](#)].
- [7] A. H. Hoang, S. Plätzer and D. Samitz, *On the Cutoff*

- Dependence of the Quark Mass Parameter in Angular Ordered Parton Showers*, *JHEP* **10** (2018) 200, [arXiv:1807.06617].
- [8] ATLAS collaboration, *Measurement of the top-quark mass in $t\bar{t} + 1$ -jet events collected with the ATLAS detector in pp collisions at $\sqrt{s} = 8$ TeV*, [arXiv:1905.02302].
- [9] CMS collaboration, *Measurement of $t\bar{t}$ normalised multi-differential cross sections in pp collisions at $\sqrt{s} = 13$ TeV, and simultaneous determination of the strong coupling strength, top quark pole mass, and parton distribution functions*, Submitted to: *Eur. Phys. J.* (2019) , [arXiv:1904.05237].
- [10] CLICDP COLLABORATION, H. Abramowicz *et al.*, *Top-Quark Physics at the CLIC Electron-Positron Linear Collider*, *JHEP* **11** (2019) 003, [arXiv:1807.02441].
- [11] M. Vos *et al.*, *Top physics at high-energy lepton colliders*, [arXiv:1604.08122].
- [12] S. Gusken, J. H. Kuhn and P. M. Zerwas, *Threshold Behavior of Top Production in e^+e^- Annihilation*, *Phys. Lett.* **B155** (1985) 185.
- [13] F. Bach, B. C. Nejad, A. Hoang, W. Kilian, J. Reuter, M. Stahlhofen *et al.*, *Fully-differential Top-Pair Production at a Lepton Collider: From Threshold to Continuum*, *JHEP* **03** (2018) 184, [arXiv:1712.02220].
- [14] A. H. Hoang, V. Mateu and S. Mohammad arjad, *Heavy Quark Vacuum Polarization Function at $\mathcal{O}(\alpha_s^2)$ and $\mathcal{O}(\alpha_s^3)$* , *Nucl. Phys.* **B813** (2009) 349, [arXiv:0807.4173].
- [15] Y. Kiyo, A. Maier, P. Maierhofer and P. Marquard, *Reconstruction of heavy quark current correlators at $\mathcal{O}(\alpha_s^3)$* , *Nucl. Phys.* **B823** (2009) 269, [arXiv:0907.2120].
- [16] A. H. Hoang and M. Stahlhofen, *The Top-Antitop Threshold at the ILC: NNLL QCD Uncertainties*, *JHEP* **05** (2014) 121, [arXiv:1309.6323].
- [17] CLICDP, CLIC collaboration, T. K. Charles *et al.*, *The Compact Linear Collider (CLIC) - 2018 Summary Report*, *CERN Yellow Rep. Monogr.* **1802** (2018) 1, [arXiv:1812.06018].
- [18] L. Linssen, A. Miyamoto, M. Stanitzki and H. Weerts, *Physics and Detectors at CLIC: CLIC Conceptual Design Report*, [arXiv:1202.5940].
- [19] P. Bambade *et al.*, *The International Linear Collider: A Global Project*, [arXiv:1903.01629].
- [20] H. Abramowicz *et al.*, *The International Linear Collider Technical Design Report - Volume 4: Detectors*, [arXiv:1306.6329].
- [21] CLIC, CLICDP collaboration, M. J. Boland *et al.*, *Updated baseline for a staged Compact Linear Collider*, [arXiv:1608.07537].
- [22] T. Barklow, J. Brau, K. Fujii, J. Gao, J. List, N. Walker *et al.*, *ILC Operating Scenarios*, [arXiv:1506.07830].
- [23] M. S. Amjad *et al.*, *A precise characterisation of the top quark electro-weak vertices at the ILC*, *Eur. Phys. J.* **C75** (2015) 512, [arXiv:1505.06020].
- [24] A. H. Hoang, A. V. Manohar, I. W. Stewart and T. Teubner, *The Threshold $t\bar{t}$ cross-section at NNLL order*, *Phys. Rev.* **D65** (2002) 014014, [hep-ph/0107144].
- [25] M. Beneke, Y. Kiyo, P. Marquard, A. Penin, J. Piclum and M. Steinhauser, *Next-to-Next-to-Next-to-Leading Order QCD Prediction for the Top Antitop S-Wave Pair Production Cross Section Near Threshold in e^+e^- Annihilation*, *Phys. Rev. Lett.* **115** (2015) 192001, [arXiv:1506.06864].
- [26] A. O. G. Kallen and A. Sabry, *Fourth order vacuum polarization*, *Kong. Dan. Vid. Sel. Mat. Fys. Med.* **29** (1955) 1.
- [27] A. Maier and P. Marquard, *Validity of Padé approximations in vacuum polarization at three- and four-loop order*, *Phys. Rev.* **D97** (2018) 056016, [arXiv:1710.03724].
- [28] A. Widl, *$t\bar{t}$ -threshold continuum matching results at $\mathcal{O}(\alpha_s^3)$* , Talk given at The 2017 International Workshop on Future Linear Colliders (LCWS2017) .
- [29] B. Dehnadi, A. H. Hoang, V. Mateu, M. Stahlhofen and A. Widl, *Threshold continuum matching for the top pair production cross section in electron-positron annihilation*, *Work in Progress*.
- [30] A. H. Hoang, Z. Ligeti and A. V. Manohar, *B decay and the Upsilon mass*, *Phys. Rev. Lett.* **82** (1999) 277, [hep-ph/9809423].
- [31] A. H. Hoang, Z. Ligeti and A. V. Manohar, *B decays in the Upsilon expansion*, *Phys. Rev.* **D59** (1999) 074017, [hep-ph/9811239].
- [32] A. H. Hoang, *1S and \overline{MS} bottom quark masses from Upsilon sum rules*, *Phys. Rev.* **D61** (2000) 034005, [hep-ph/9905550].
- [33] A. H. Hoang, A. Jain, I. Scimemi and I. W. Stewart, *Infrared Renormalization Group Flow for Heavy Quark Masses*, *Phys. Rev. Lett.* **101** (2008) 151602, [arXiv:0803.4214].
- [34] A. H. Hoang, A. Jain, C. Lepenik, V. Mateu, M. Preisser, I. Scimemi *et al.*, *The MSR Mass and the $\mathcal{O}(\Lambda_{QCD})$ Renormalon Sum Rule*, [arXiv:1704.01580].
- [35] M. Beneke, P. Marquard, P. Nason and M. Steinhauser, *On the ultimate uncertainty of the top quark pole mass*, *Phys. Lett.* **B775** (2017) 63, [arXiv:1605.03609].
- [36] A. H. Hoang, C. Lepenik and M. Preisser, *On the Light Massive Flavor Dependence of the Large Order Asymptotic Behavior and the Ambiguity of the Pole Mass*, *JHEP* **09** (2017) 099, [arXiv:1706.08526].
- [37] M. B. Voloshin, *'Optical' sum rule for form-factors of heavy mesons*, *Phys. Rev.* **D46** (1992) 3062.
- [38] A. Hoang, P. Ruiz-Femenia and M. Stahlhofen, *Renormalization Group Improved Bottom Mass from Upsilon Sum Rules at NNLL Order*, *JHEP* **10** (2012) 188, [arXiv:1209.0450].
- [39] M. Boronat, J. Fuster, I. Garcia, P. Roloff, R. Simoniello and M. Vos, *Jet reconstruction at high-energy electron-positron colliders*, *Eur. Phys. J.* **C78** (2018) 144, [arXiv:1607.05039].
- [40] T. Suehara and T. Tanabe, *LCFIPlus: A Framework for Jet Analysis in Linear Collider Studies*, *Nucl. Instrum. Meth.* **A808** (2016) 109, [arXiv:1506.08371].
- [41] M. Sohail Amjad, *Forward-Backward asymmetry in top pair production at the ILC*. PhD thesis, Orsay, LAL, 2014 [electronic copy].
- [42] K. Kawagoe *et al.*, *Beam test performance of the highly granular SiW-ECAL technological prototype for the ILC*, [arXiv:1902.00110].
- [43] ILD CONCEPT GROUP, T. Abe *et al.*, *The International Large Detector: Letter of Intent*, [arXiv:1006.3396].
- [44] CLICDP COLLABORATION, D. Arominski *et al.*, *A detector for CLIC: main parameters and performance*, [arXiv:1812.07337].

- [45] J. S. Marshall and M. A. Thomson, *Pandora Particle Flow Algorithm*, in *Proceedings, International Conference on Calorimetry for the High Energy Frontier (CHEF 2013): Paris, France, April 22-25, 2013*, 305, 2013. [[arXiv:1308.4537](#)].
- [46] CALICE collaboration, C. Adloff et al., *Response of the CALICE Si-W electromagnetic calorimeter physics prototype to electrons*, *Nucl. Instrum. Meth.* **A608** (2009) 372, [[arXiv:0811.2354](#)].
- [47] M. Boronat, *Development of the quality test protocol for the DEPFET pixel detectors and top-quark mass measurement at high energy e^+e^- colliders*, *Ph.D. thesis U. Valencia* (2017) [[electronic copy](#), CERN thesis [CERN-THESIS-2017-479]].
- [48] CLIC collaboration, J. J. Blaising, D. Dannheim and A. Sailer, *In-situ detector calibration at CLIC*, [[CLICdp-Note-2019-003](#)].
- [49] ATLAS collaboration, *Electron and photon energy calibration with the ATLAS detector using 2015–2016 LHC proton-proton collision data*, *JINST* **14** (2019) P03017, [[arXiv:1812.03848](#)].
- [50] CMS collaboration, *Performance of Photon Reconstruction and Identification with the CMS Detector in Proton-Proton Collisions at $\sqrt{s} = 8$ TeV*, *JINST* **10** (2015) P08010, [[arXiv:1502.02702](#)].
- [51] D. Schulte, *Beam-Beam Simulations with GUINEA-PIG*, [CERN-PS-99-014-LP].
- [52] S. Poss and A. Sailer, *Luminosity spectrum reconstruction at linear colliders*, *Eur. Phys. J.* **C74** (2014) 2833.
- [53] D. Arominski, E. Fullana, J. Fuster, P. Gomis, M. Vos and A. Sailer, *Determination of the CLIC luminosity spectrum at 380 GeV*, *Work in progress*.
- [54] G. Rodrigo, A. Santamaria and M. S. Bilenky, *Do the quark masses run? Extracting $m\text{-bar}(b)$ ($m(z)$) from LEP data*, *Phys. Rev. Lett.* **79** (1997) 193, [[hep-ph/9703358](#)].
- [55] DELPHI collaboration, P. Abreu et al., *$m(b)$ at $M(Z)$* , *Phys. Lett.* **B418** (1998) 430.
- [56] A. Gizhko et al., *Running of the Charm-Quark Mass from HERA Deep-Inelastic Scattering Data*, *Phys. Lett.* **B775** (2017) 233, [[arXiv:1705.08863](#)].
- [57] CMS collaboration, *Running of the top quark mass from proton-proton collisions at $\sqrt{s} = 13$ TeV*, [[arXiv:1909.09193](#)].
- [58] C. Farrell and A. H. Hoang, *Next-to-leading-logarithmic QCD corrections to the cross-section $\sigma(e^+e^- \rightarrow t\bar{t}H)$ at 500 GeV*, *Phys. Rev.* **D74** (2006) 014008, [[hep-ph/0604166](#)].
- [59] C. Farrell and A. H. Hoang, *The Large Higgs energy region in Higgs associated top pair production at the linear collider*, *Phys. Rev.* **D72** (2005) 014007, [[hep-ph/0504220](#)].